DOI: 10.3901/CJME.2014.1021.159, available online at www.springerlink.com; www.cjmenet.com; www.cjmenet.com.cn

Analysis of the Pump-turbine S Characteristics Using the Detached Eddy Simulation Method

SUN Hui[1], XIAO Ruofu[1,*], WANG Fujun[1], XIAO Yexiang[2], and LIU Weichao[3]

1 *College of Water Resources and Civil Engineering, China Agricultural University, Beijing 100083, China*
2 *State Key Laboratory of Hydroscience and Engineering & Department of Thermal Engineering, Tsinghua University, Beijing 100083, China*
3 *Dongfang Electric Machinery Co., Ltd, Deyang 618000, China*

Received July 9, 2013; revised June 9, 2014; accepted October 21, 2014

Abstract: Current research on pump-turbine units is focused on the unstable operation at off-design conditions, with the characteristic curves in generating mode being S-shaped. Unlike in the traditional water turbines, pump-turbine operation along the S-shaped curve can lead to difficulties during load rejection with unusual increases in the water pressure, which leads to machine vibrations. This paper describes both model tests and numerical simulations. A reduced scale model of a low specific speed pump-turbine was used for the performance tests, with comparisons to computational fluid dynamics(CFD) results. Predictions using the detached eddy simulation(DES) turbulence model, which is a combined Reynolds averaged Naviers-Stokes(RANS) and large eddy simulation(LES) model, are compared with the two-equation turbulence mode results. The external characteristics as well as the internal flow are for various guide vane openings to understand the unsteady flow along the so called S characteristics of a pump-turbine. Comparison of the experimental data with the CFD results for various conditions and times shows that DES model gives better agreement with experimental data than the two-equation turbulence model. For low flow conditions, the centrifugal forces and the large incident angle create large vortices between the guide vanes and the runner inlet in the runner passage, which is the main factor leading to the S-shaped characteristics. The turbulence model used here gives more accurate simulations of the internal flow characteristics of the pump-turbine and a more detailed force analysis which shows the mechanisms controlling of the S characteristics.

Keywords: pump-turbine, S-shaped characteristics, detached eddy simulation(DES), numerical analysis

1 Introduction

Pumped storage power stations have good flow dynamics and provide high-quality economical energy. Thus, the growing demand for better power balancing and frequency control is resulting in the use of more pumped storage units. Reversible pump-turbines in many cases are the most cost-effective solution.

For pump-turbine units operating in the S shaped operating characteristics region, some speeds correspond to three different flow conditions with a positive slope along the operating line which results in both positive and negative torques which can easily damage the pump-turbine components[1]. During turbine startup and synchronization, such instabilities must be avoided with faster startup and switch-over times needed in today's very dynamic electricity markets.

The S characteristics of pump-turbine operations were first pointed out by TANAKA, et al[2]. Since the S characteristics of pump-turbine units are very important, there have been many studies of this problem. HASMATUCHI, et al[3–4], measured the flow characteristics using the PIV method with a numerical investigation of a scale model pump-turbine model at off-design operating conditions in the generating mode. Recent publications, such as WIDMER, et al[5], showed that the S-shaped curve can be traced back to flow recirculation and vortex formation within the runner and the vaneless space between the runner and guide vanes. XIAO, et al[6–7], pointed out that misaligned guide vanes can eliminate the S characteristics for steady flow. However, pre-opening of the guide vanes increased the flow rate for the runaway condition and destroyed the flow symmetry in the runner, which increased the pressure pulsations and resulted in unstable unit operation.

The detached eddy simulation (DES) model was first proposed by SPALART[8–9] in 1997 and first used in 1999. His papers gave a detailed introduction of the relationship between the DES model and the LES/RANS models. GEORGE, et al[10], used the large eddy simulation (LES) method and the DES model to investigate the flow around a

* Corresponding author. E-mail: xrf@cau.edu.cn
Supported by National Natural Science Foundation of China (Grant No. 51139007), and State Key Laboratory of Hydroscience and Engineering Open Foundation of China (Grant No. 2014-KY-05)

sphere. DES model has also been successfully used in recent years to analysis a variety of complex models with many recent studies showing that the DES model gives more accurate results than the two-equation turbulence model when significant flow separation occurs within the flow field[11–13].

This study focuses on predicting the unsteady flow near runaway of a pump-turbine unit using the DES model and on the internal flow characteristics as well as the force characteristics leading to the S characteristics instability.

2 Experimental Setup

This study used a reduced scale model of the low specific speed pump-turbine shown in Fig. 1, which was installed in the hydraulic testing hall in the Dongfang Electric Machinery Co., Ltd. The unit had 9 blades rotating in a 20 wicket gate distributor. The inlet diameter, D_{in}, of the spiral case was 330 mm and the outlet diameter, D_{out}, of the draft tube was 650 mm. The experimental setup is shown in Fig. 2.

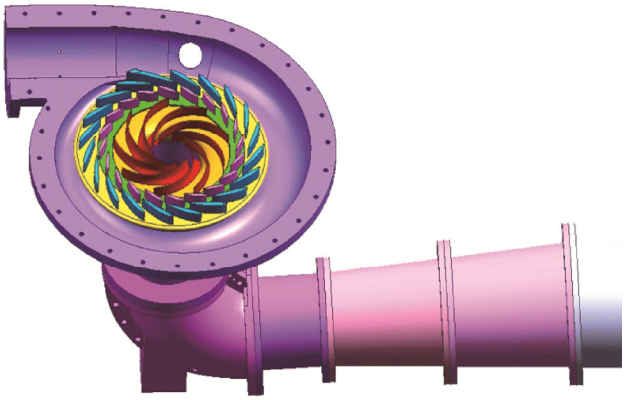

Fig. 1. Reduced scale pump-turbine model

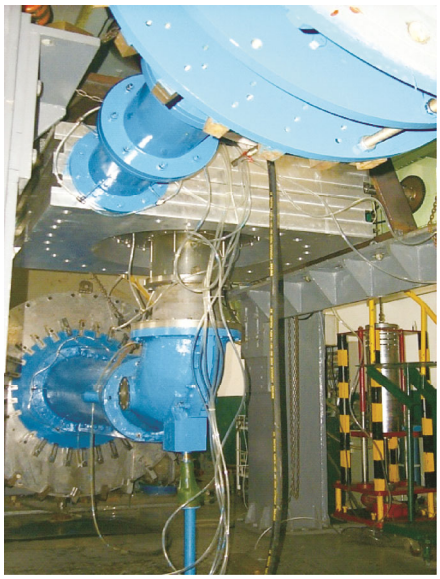

Fig. 2. Experimental setup for model measurements

The turbine operating conditions and the braking condition were investigated since they involve the S shaped region. The specific monitoring data was as follows:

Δp—Pressure drop monitored by a differential pressure sensor,

Q—Mass flow rate monitored by a flow sensor located in the outlet pipe,

N, M—Nominal rotational speed and torque monitored by an electromagnetic torque meter.

The head was defined as

$$H = \frac{\Delta p}{\rho g} + \frac{v_1^2 - v_2^2}{2g}, \tag{1}$$

where

$$v_1 = \frac{4Q}{\pi D_{in}^2}, \quad v_2 = \frac{4Q}{\pi D_{out}^2}. \tag{2}$$

3 Simulation Model and Mesh

3.1 Simulation model

The simulations included the entire flow passage in the pump-turbine, including the spiral case, stay vanes, guide vanes, runner and draft tube. The pump turbine components are shown in Fig. 3, with the pump-turbine specifications listed in Table 1.

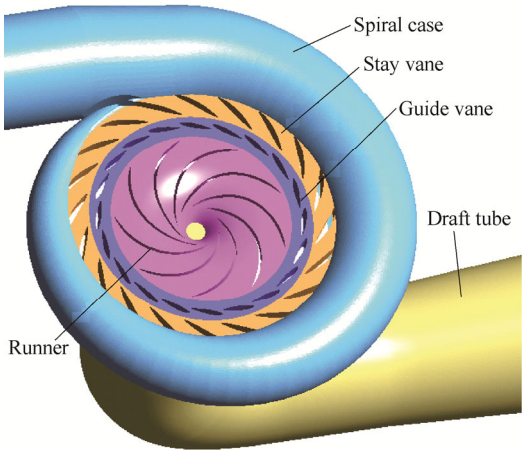

Fig. 3. Pump-turbine components

Table 1. Pump-turbine characteristics

Parameter	Value
Number of runner blades Z_r	9
High-pressure side runner diameter D_1/mm	515.4
Low-pressure side runner diameter D_2/mm	300
Rotational speed n/(r • min^{-1})	1200
Number of guide vanes Z_1	20
Number of stay vanes Z_2	20

3.2 Mesh

The present study used ANSYS-CFX 14.0 for the calculations, with the transport equations solved by the finite volume method. The first step in the numerical simulations was to generate the mesh. Since the pump-turbine internal flow is very complex, a very detailed

high quality mesh was needed in the entire flow passage to capture the basic factors affecting the S characteristics. The mesh divisions were very important for both the CFD calculations and the result analysis.

The mesh in the runner region was generated using the commercial software TurboGrid, while the rest was generated using the commercial software ICEM/CFD 14.0. Since the spiral case surface has no sharp corners and the curvature changes only a little, a tetrahedral mesh was used with a boundary layer mesh to eliminate prismatic elements near the wall to better simulate the flow in the boundary layers. A hexahedral mesh was used in the stay vanes, guide vanes, runner and draft tube regions for better mesh quality. Two different turbulence models were used with the mesh appropriate for both turbulence models. Grid independence checks for steady flow used five different mesh sizes with from 600 000 to 1 500 000 nodes. The numerical simulations show that the results are more accurate with smaller elements size. The differences in the computed results with different grids were less than 0.2% with meshes having more than 1 500 000 nodes. The mesh with 1 500 000 nodes was then used. For unsteady conditions, the mesh had to be quite dense around the guide vanes and the runner, with a grid independence study resulting in 3 000 000 nodes with the mesh shown in Fig. 4.

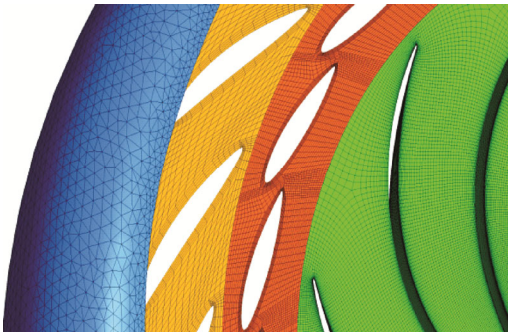

Fig. 4. Part of the computational mesh for the unsteady flow field

4 Turbulence Model and Boundary Conditions

4.1 Turbulence model

The three main strategies used for turbulent flow simulations are direct numerical simulations(DNS), Reynolds averaged Naviers-Stokes(RANS) and LES models. The DNS method is not practical due to the massive computational resources required to resolve all the length and time scales in the turbulent flow spectrum. The RANS models are widely used in industrial applications since they require relatively small computational resources due to the ensemble-averaging of the governing equations. While the RANS method models model all the turbulence scales, which often fail to provide accurate results for complex flows since the large turbulence scales for separated flows are strongly dependent on the geometry[14]. Large eddy simulations divide all the variables in the flow field into large scale variables and small scale variables through a filtering function. The large scales are resolved, which the small scales are modeled. Lattice Boltzmann methods can also be used with the appropriate egalitarian functions. The wall-modeled LES (WMLES) method provides very good results (at smaller computational costs than the usual (wall-resolved) LES), but the numerical requirements are expensive compared to RANS models. The WMLES uses the RANS model for the very near wall layer[15].

The primary advantage of the DES method is that it can be applied at high Reynolds numbers (as can Reynolds-averaged techniques) but also resolves geometry-dependent, unsteady three-dimensional turbulent motion as in the LES model. The DES model combines the advantages of the RANS and LES models and, thus, has the potential to offer more accuracy than RANS at less cost than LES[16–17]. The main idea is that the Reynolds averaged N-S equations are used near the wall while the LES method is used to calculate large separation flows. This takes advantage of the smaller number of calculations with the Reynolds averaging method in the boundary layer and overcomes the shortcomings of the LES that is too demanding of the mesh near the wall at high Reynolds numbers to give better results.

This analysis used the DES method based on the SST to simulate the internal flow conditions for the pump-turbine S characteristics. The SST $k-\omega$ turbulence equation is:

$$\frac{\partial(\rho k)}{\partial t}+u_i\frac{\partial(\rho k)}{\partial x_i}=P_k-\frac{\rho k^{3/2}}{l_{k-\omega}}+\frac{\partial}{\partial x_i}\left[\left(\mu_l+\frac{\mu_t}{\sigma_k}\right)\frac{\partial k}{\partial x_i}\right], \quad (3)$$

$$\frac{\partial(\rho\omega)}{\partial t}+u_i\frac{\partial(\rho\omega)}{\partial x_i}=C_\omega P_\omega-\beta_\omega\rho\omega^2+\frac{\partial}{\partial x_i}\left[\left(\mu_l+\frac{\mu_t}{\sigma_k}\right)\frac{\partial k}{\partial x_i}\right]+2\rho(1-F_1)\frac{1}{\sigma_{\omega 2}}\frac{1}{\omega}\frac{\partial k}{\partial x_i}\frac{\partial\omega}{\partial x_i}, \quad (4)$$

where P_k and P_ω are the turbulence generation and dissipation source terms and F_1 and F_2 are mixed functions.

The eddy viscosity coefficient is

$$\mu_t=\min\left[\frac{\rho k}{\omega},\frac{a_1\rho k}{\Omega F_2}\right]. \quad (5)$$

The turbulence scale parameter in the dissipative term of the k equation is

$$l_{k-\omega}=k^{1/2}\beta_k\omega. \quad (6)$$

In the DES method, the turbulence scale $l_{k-\omega}$ is replaced by $\min(l_{k-\omega}, C_{\mathrm{DES}}\Delta)$, where Δ is the grid scale which for a heterogeneous grid $\Delta=\max(\Delta x,\Delta y,\Delta z)$, the maximum side length in the mesh, and the constant $C_{\mathrm{DES}}=0.65$. In

the boundary layer near the walls, $l_{k-\omega} \leqslant C_{\mathrm{DES}}\Delta$ and the model switches to the SST $k-\omega$ turbulence model. Away from the wall, $l_{k-\omega} > C_{\mathrm{DES}}\Delta$ and the model uses the Subgrid Reynolds Stress Model in the large eddy simulation method[18–19].

4.2 Boundary conditions

Steady simulations were performed with the SST $k-\omega$ two equation model and the unsteady simulations with the DES model using the steady-state results as the initial data.

The inlet boundary condition was a constant flow rate into the spiral case with the outlet condition being an averaged relative pressure of 0 Pa at the draft tube outlet. The no-slip condition was used on all the solid walls, with the standard wall functions used to calculate the turbulence kinetic energy and turbulence dissipation near the wall. The general grid interface(GGI) method was used to connect the meshes in the different domains.

The transient simulations used a time step of 1/100 of the rotation period (Δt=0.000 5 s) with the total time including 20 rotations.

5 CFD Calculations

5.1 External characteristic results

Numerical simulations were performed with guide vane openings of 6° and 8°, with 10 simulation points for each opening, the results are reported as follows:

$$Q_{11}=\frac{Q}{D_1^2\sqrt{H}},\quad n_{11}=\frac{nD_1}{\sqrt{H}},\quad M_{11}=\frac{M}{D_1^3H},\tag{7}$$

where n_{11} is the unit speed, Q_{11} is the unit flow, M_{11} is the unit torque, Q is the mass flow rate, H is the head, and D_1 is the runner diameter.

The calculated results are shown in Fig. 5. Comparison of the experimental data and calculated results for the two different turbulence models shows that the basic trends of the predictions agree well with the experimental data. The good agreement between the CFD simulations and the experimental data shows that the simulations can provide accurate results that can be used to identify the internal flows for runaway conditions. The relative errors of the unsteady DES predictions are smaller than those of the steady-state simulations using the two equation turbulence model, especially in the low flow region near the runaway operating condition. The characteristic curve given by the DES model agrees well with the experimental data, so the flow characteristics in the pump-turbine close to runaway should be well predicted by the unsteady DES turbulence model. Thus, this is a very good foundation for further analyses of the internal flow field to explain the S characteristics.

The characteristic operating curve for the unit flow, Q_{11}, bends rapidly downward in Fig. 5, becomes vertical and even reverses to form the S shape. Since pumped storage power stations require frequent load changes, if the operating conditions enter the S shaped region, the flow instabilities can affect the safety of the entire unit. These instabilities will result in positive and negative torques that can easily destroy the pump-turbine unit.

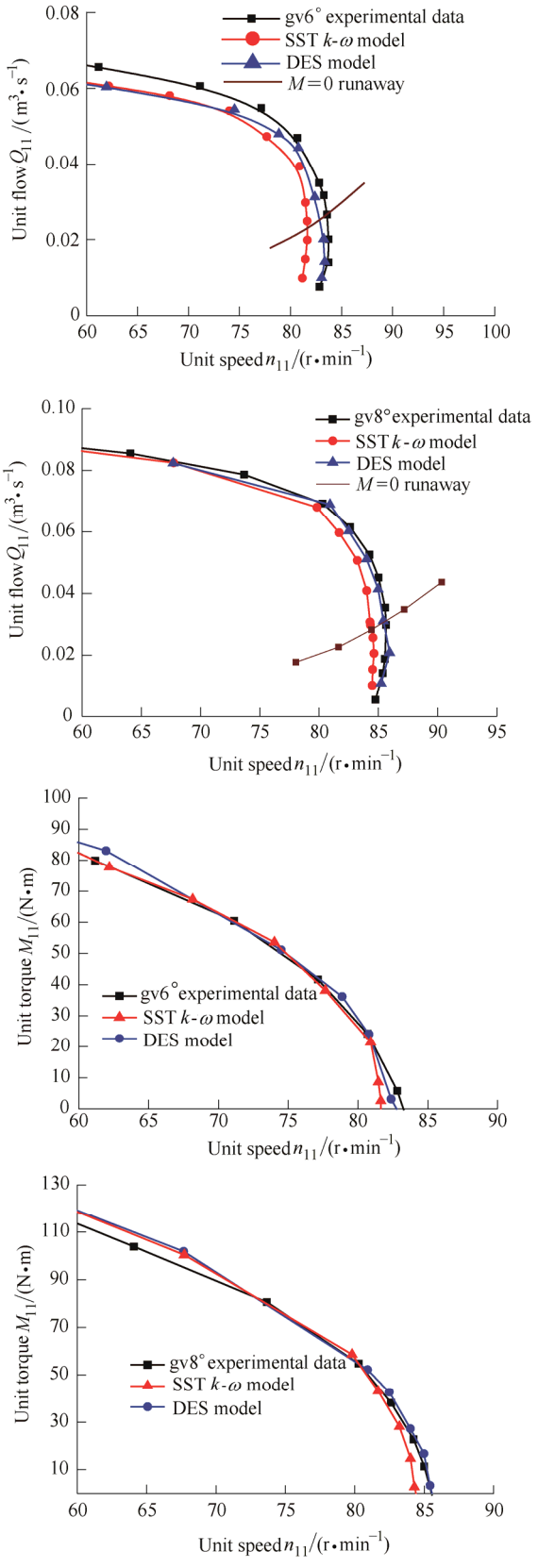

Fig. 5. Comparisons of the results of the two turbulence models with experimental data

In addition, the angle between the characteristic curve and the runaway line is very small. Thus, since the slope of the characteristics curve at the intersection is positive, the operating condition can easily go into the braking zone without a smooth transition.

5.2 Internal flow analysis

The internal flow characteristics were analyzed for six operating conditions to investigate the reasons for the S-shaped curve characteristics for the 8° opening as shown in Fig. 6, where P_5 is the runaway condition point, P_6 is slightly below the runaway point and the other four are all above the runaway point. P_2 is the turning point in the characteristics curve with the unit flow Q_{11} decreasing rapidly as shown in Fig. 6.

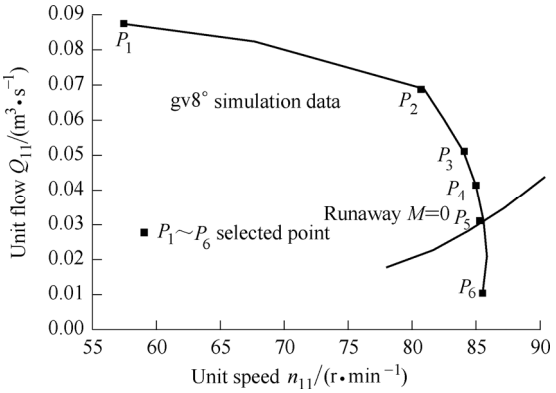

Fig. 6. Six operating points used to investigate the flow field

Fig. 7 shows the radial velocities for each of the six operating points along the span normalized on the hub to shroud line of the runner inlet. The vertical axis represents the dimensionless relative distance from hub to shroud. The low flow conditions (P_3, P_4, P_5 and P_6) have both positive and negative radial velocities which the flows at P_1 and P_2 with relatively large flow rates having only inlet flow.

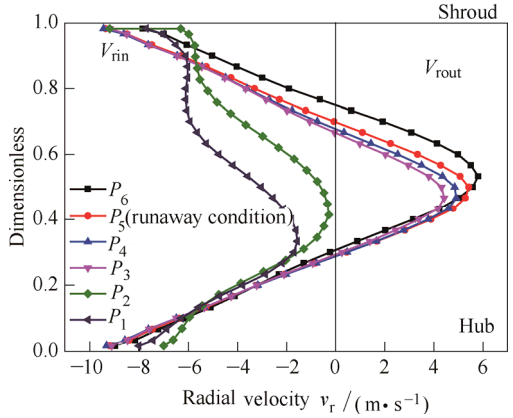

Fig. 7. Normalized radial velocities on the hub to shroud line

The three dimensional inlet to the runner is defined as surface S in Fig. 8. The flow rate can be calculated as

$$q = \int_s \vec{v}_n \mathrm{d}s, \tag{8}$$

where v_n includes v_{in} and v_{out}, and

$$q_{in} = \int_S v_{in} \mathrm{d}s,\ q_{out} = \int_S v_{out} \mathrm{d}s. \tag{9}$$

The absolute value of the flow is

$$q_{abs} = q_{in} - q_{out}. \tag{10}$$

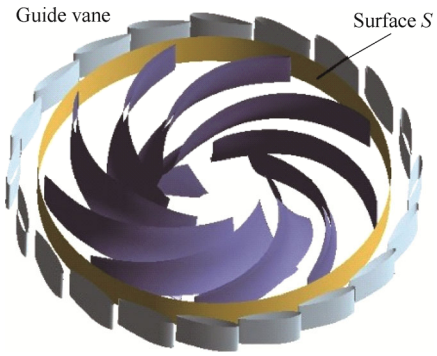

Fig. 8. Inlet surface of the runner

Fig. 9 shows the axial velocities at the leading edge of the runner for the P_1 and P_5 conditions. The P_1 condition has almost no backflow at the leading edge so the flow will enter the runner with a smaller energy loss. However, the runaway condition, P_5, has a large backflow in the runner channel in front of the leading edge, with the back flow blocking the flow and reducing the flow into the runner. The backflow is related to the unstable flow in the S-shaped pump-turbine operating region.

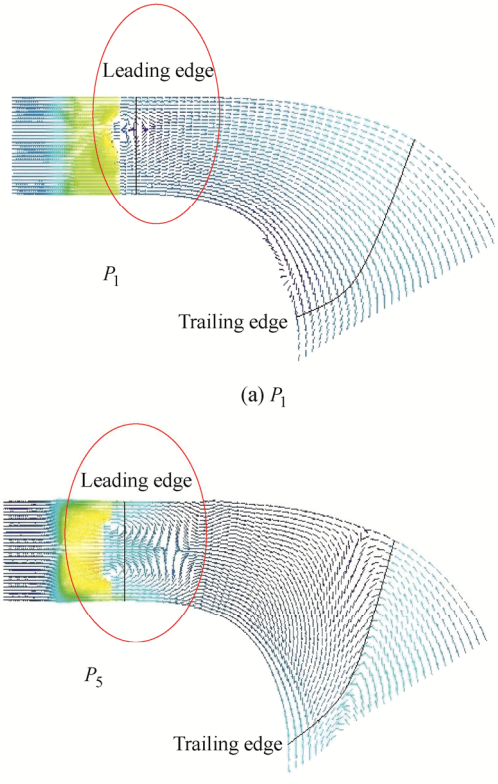

Fig. 9. Axial velocity vectors at the leading edge

Fig. 10 shows the distribution of the radial velocities flowing inward and outward at the runner inlet, which leads to the formation of vortices in the runner passages and along the entire leading edge at the runaway operating point, P_5. A large amount of energy is dissipated between the guide vanes and the runners causing large differences between the inward and outward energy fluxes through surface S at the runaway operating condition.

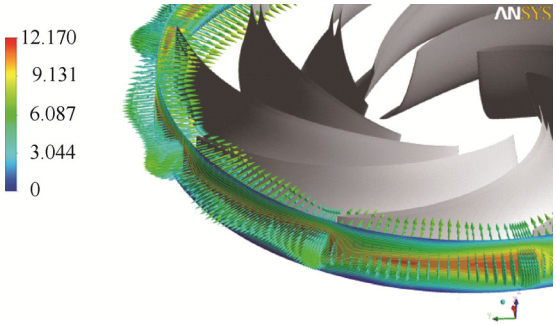

Fig. 10. Velocity meridional vectors at the runner inlet (m/s)

The streamlines in the runner for the P_5, P_2 and P_1 conditions are shown in Fig. 11. Normal flow separation occurs at the low flow condition as shown in part (c), while the P_2 condition is where the flow rate decreases to the turning point of the characteristic curve with flow separation in the runner inlet. The flow rate is further reduced at the P_5 runaway condition with a large number of vortices in the runner domain with back flow blocking the flow.

5.3 Force analysis

In a rotating frame of reference attached to the runner, the pressure gradient perpendicular to the inviscid, one-dimensional main flow along a streamline is the balance of the equilibrium forces caused by the following accelerations.

Centrifugal acceleration due to rotation is

$$a_{z,R} = \omega^2 \cdot r. \tag{11}$$

Centrifugal acceleration due to streamline curvature is

$$a_{z,SL} = \frac{v_r^2}{R_{SL}}. \tag{12}$$

Coriolis forces are

$$a_c = 2 \cdot \omega \times v_r. \tag{13}$$

The radial equilibrium equation was expressed by BERTEN[20] as

$$\frac{1}{\rho}\frac{\partial p}{\partial n} = 2 \cdot \omega \times v_r + r \cdot \omega^2 \frac{\partial r}{\partial n} - \frac{v_r^2}{R_{SL}}. \tag{14}$$

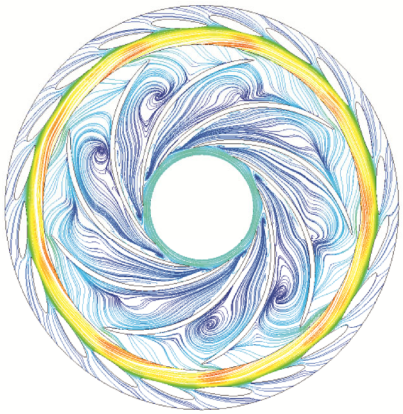

(a) P_5 (runaway)

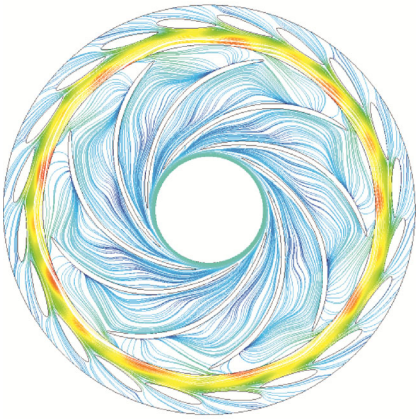

(b) P_2

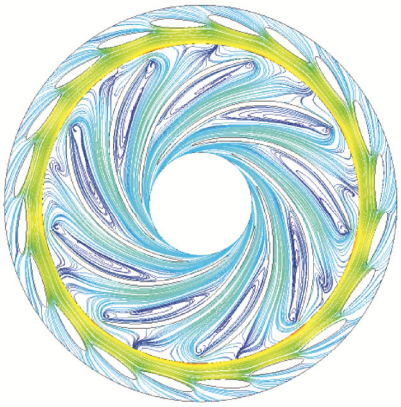

(c) P_1

Fig. 11. Streamlines in the runner for various conditions

Fig. 12 illustrates the accelerations for a fluid element in the rotating runner channel of a pump-turbine and a traditional low specific speed turbine.

In traditional low specific speed turbines, the angle of the high pressure side of the blade is close to 90° as shown in Fig. 12(b), so the centrifugal acceleration due to the streamline curvature is small, which makes the total centrifugal force small. However, for the pump-turbine the centrifugal force is large which restricts the flow entering the runner and creates a recirculation vortex in front of the runner inlet as the main reason for the S characteristics.

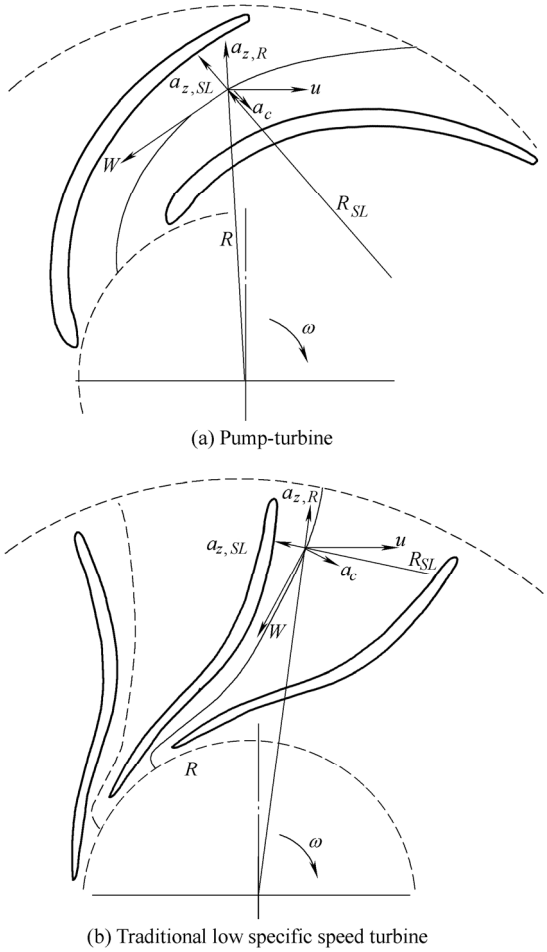

Fig. 12. Velocities and resulting accelerations for a fluid element in the runner channel

That is one of the reasons for the large centrifugal force in the pump-turbine. The problem is that the best efficiency points for the turbine and pump conditions do not coincide, so the pump-turbine is designed as a pump and checked as a turbine. As a result, the unit speeds, n_{11}, for the operating range of the pump unit are higher than those of the best efficiency point of the turbine model, so the turbine operates at partial load conditions. For a traditional hydraulic turbine the specific speed, n_s, at the best efficiency point is higher than that for a pump-turbine unit as shown in Fig. 13.

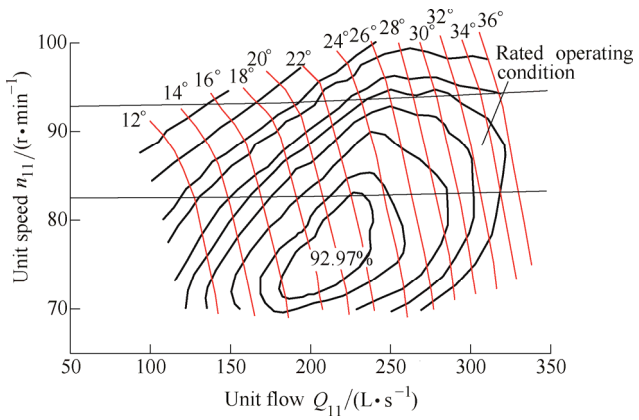

Fig. 13. Model characteristic curve

According to basic fluid machinery theory, a lower pump-turbine specific speed means that the runner flow passage is longer and the high-pressure side diameter, D_1, of the pump-turbine should be greater than that of the traditional turbine to increase the centrifugal force in the runner. A wide range of designs show that the diameters of the pump-turbines are 1.4–1.45 times than those of traditional turbines[21].

Thus, the large centrifugal force of the pump-turbine runner results from these two mechanisms. Another reason for the recirculation flow near the rotor inlet is the great inconsistency between the inflow angle and the inlet blade angle, so the incident angle is very large as shown in Fig. 12.

6 Conclusions

(1) The pump-turbine flow and operating characteristics can be well predicted by CFD simulations using DES model.

(2) The unstable flow fields were predicted in the so called S-shaped portion of the characteristic curve. The internal flows that reduce Q_{in} at the runner inlet are due to unbalanced distributions of the inward and outward flowing radial velocities which leads to the S shaped operating characteristics.

(3) The main reasons for the reduced mass flow rate are the streamline curvature of the flow in the pump-turbine which is larger than in a traditional low specific speed turbine and the large centrifugal force prevents some flow from entering the runner. The restricted flow into the runners leads to formation of vortices in the vaneless space between the guide vanes and the runners. Therefore, the large centrifugal force and the vortices are then the cause of the instabilities that cause the S shaped operating characteristics.

References

[1] MEI Zuyan. *Pumped storage technology*[M]. Beijing: Tsinghua University Press, 1986. (in Chinese)

[2] TANAKA H, TSUNODA S. The development of high head single stage pump-turbines[C]//*Proceedings of 10th IAHR Symposium on Hydraulic Machinery and Cavitation*, Tokyo, Japan, 1980: 429–440.

[3] HASMATUCHI V, ROTH S, BOTERO F, et al. High-speed flow visualization in a pump-turbine under off-design operating conditions[C]//*IOP Conference Series: Earth and Environmental Science*, IOP Publishing, 2010, 12(1): 012059.

[4] HASMATUCHI V, FARHAT M, ROTH S, et al. Experimental evidence of rotating stall in a pump-turbine at off-design conditions in generating mode[J]. *Journal of Fluids Engineering*, 2011, 133(5): 051104.

[5] WILDMER C, STAUBLI T, LEDERGERBER N. Unstable characteristic and rotating stall in turbine brake operation of pump-turbines[J]. *Journal of Fluids Engineering-Transactions of the ASME*, 2011, 133(1): 041101.

[6] XIAO Ruofu, SUN Hui, LIU Weichao, et al. The analysis of S characteristics and its pressure pulsation of pump-turbine under Pre-opening guide vanes[J]. *Journal of Mechanical Engineering*, 2012, 48(8): 174–179. (in Chinese)

[7] SUN Hui, XIAO Ruofu, LIU Weichao, et al. Analysis of S characteristics and pressure pulsations in a pump-turbine with misaligned guide vanes[J]. *Journal of Fluids Engineering-Transactions of the ASME*, 2013, 135(5): 051101.
[8] SPALART P R. Strategies for turbulence modeling and simulations[J]. *International Journal of Heat Fluid Flow*, 2000, 21(3): 252–263.
[9] SPALART P R. Young person's guide to detached-eddy simulation grids[G]. *Technical Report* CR-2001-211032, NASS.
[10] CONSTANTINESCU S G, SQUIRES K D. *LES and DES investigations of turbulent flow over a sphere*[M]. American Institute of Aeronautics and Astronautics, 2000.
[11] LI Guojing, DAI Guangqing, YANG Qing, et al. Detached eddy simulation of hydraulic characteristics along the side-wall after a new arrangement-scheme of the sudden lateral enlargement and the vertical drop[J]. *Journal of Hydrodynamics*, 2011, 23(5): 669–675.
[12] MOHAMMAD F A, KEITH D, DAVID S T. A new hybrid RANS/LES modeling methodology for CFD applications[C/CD]// *Proceeding of the ASME-JSME-KSME Joint Fluids Engineering Conference*, Hamamatsu, Japan, July 24–29, 2011.
[13] MENTER F R, KUNTZ M, BENDER R. A scale-adaptive simulation mode using two-equation models[G]. *AIAA Paper* 2003-0767.
[14] FORSYTHE J R, HOFFMANN K A, CUMMINGS R M, et al. Detached-eddy simulation with compressibility corrections applied to a supersonic axisymmetric base flow[J]. *Journal of Fluids Engineering*, 2002, 124: 911–923.
[15] SHUR M L, SPALART P R, STRELETS M K, et al. A hybrid RANS-LES approach with delayed-DES and wall-modelled LES capabilities[J]. *International Journal of Heat and Fluid Flow*, 2008, 29(6): 1638–1649.
[16] SLIMON S. Computation of internal separated flows using a zonal detached eddy simulation approach[C/CD]//*Proceedings of the 2003 ASME International Mechanical Engineering Congress*, Washington, DC, USA, 2003.
[17] DAVIDSON L, BILLSON M. Hybrid LES-RANS using synthesized turbulent fluctuations for forcing in the interface region[J]. *International Journal of Heat and Fluid Flow*, 2006, 27(6): 1028–1042.
[18] MISRA A, PULLIN D I. A vortex-based subgrid stress model for large-eddy simulation[J]. *American Institute of Physics*, 1997, 9(8): 2444–2454.
[19] STRELETS M. Detached eddy simulation of massively separated flows[G]. *AIAA Pape*r, 2001-0897.
[20] BERTEN S. Hydrodynamics of high specific power pumps for off-design operating conditions[D]. Lausanne, Switzerland: EPFL, 2010.
[21] MEI Zuyan. *Pumped storage power generation technology*[M]. Beijing: Mechanical Industry Press, 2000. (in Chinese)

Biographical notes

SUN Hui, born in 1988, is currently a master candidate at *College of Water Resources and Civil Engineering, China Agricultural University, China.*
E-mail: sh0929@163.com

XIAO Ruofu, born in 1976, is currently an associate professor and a PhD candidate supervisor at *College of Water Resources and Civil Engineering, China Agricultural University, China*. He received his PhD degree from *Huazhong University of Science and Technology*, *China*, in 2004. His research interests include hydraulic machinery and Fluid-structure interaction.
Tel: +86-10-62736578; E-mail: xrf@cau.edu.cn

WANG Fujun, born in 1964, is currently a professor and a PhD candidate supervisor at *College of Water Resources and Civil Engineering, China Agricultural University, China.*
E-mail: wangfj@cau.edu.cn

XIAO Yexiang, born in 1978, is currently an associate professor at *State Key Laboratory of Hydroscience and Engineering* & *Department of Thermal Engineering, Tsinghua University, China*.
E-mail: xiaoyex@mail.tsinghua.edu.cn

LIU Weichao, born in 1973, is currently an engineer at *Dongfang Electric Machinery Co., Ltd, China.*
E-mail: hustlwc@163.com